Title: Does manganese influence grass litter decomposition on a Hawaiian rainfall gradient?

Elizabeth L. Paulus*[1], Peter M. Vitousek[2]

[1]Stanford Synchrotron Radiation Lightsource, SLAC National Accelerator Laboratory, Menlo Park, California 94025 USA; [2]Stanford University Department of Earth System Science, Yang and Yamazaki Environment and Energy Bldg 140, 437 Via Ortega, Stanford, California 94305 USA

*Corresponding author: paulus@stanford.edu

Abstract

Plant litter is a well-defined pool of organic matter (OM) in which the influence of manganese (Mn) on decomposition (both decomposition rate, and the mix of compounds ultimately transferred to soil OM) has been clearly demonstrated in temperate forests. However, no similar study exists on grasslands, and the effect of foliar Mn versus soil-derived Mn on litter decomposition is poorly known. We used 5-month and 12-month field and 10-month laboratory experiments to evaluate litter decomposition on the Kohala rainfall gradient (Island of Hawai‘i) in areas with different foliar and soil Mn abundances, and on which a single plant species (*Pennisetum clandestinum*) dominates primary production and the litter pool. Chemical imaging analyses of decomposed litter revealed that Mn^{2+} oxidized to Mn^{3+} and Mn^{4+} on grass litter during decompositions—hallmarks of Mn-driven litter oxidation. However, these transformations and Mn abundance did not predict greater litter mass loss through decomposition. These observations demonstrate that the importance of Mn to an ecosystem's C cycle does not rely solely on the metal's abundance and availability.

Keywords: manganese, organic carbon, grassland, redox cycling, litter decomposition

1. Introduction

In natural and laboratory environments within temperate forests, manganese (Mn) abundance and availability correlate with litter decay (Cui and Dolphin 1990; Berg and McClaugherty 2003; Berg et al. 2007; Davey et al. 2007; Keiluweit et al. 2015; Whalen et al. 2018). A comprehensive literature review found Mn concentration so highly correlated with degree of decomposition that it appears to be "the single main factor" predicting OM decay in many sites (Berg et al. 2010). In

this study, we investigate whether Mn influences grassland litter decomposition and whether the Mn source—foliar or soil—matters.

Mn is a biologically essential element ubiquitous in soil. In natural environments, it exists in three oxidation states: Mn^{2+} is the most reduced, energetically stable, soluble species and the only nutritionally available (or bioavailable) form; Mn^{4+} is the most oxidized and least soluble form; and Mn^{3+}, a powerful and unstable oxidant, is the most reactive form (van der Lee 1999; Rezanezhad et al. 2014; Keiluweit et al. 2016; Jones et al. 2018). Due to the thermodynamics of the single-electron oxidation or reduction step required to produce Mn^{3+} from Mn^{2+} or Mn^{4+}, Mn^{3+} is an extremely unlikely intermediate between Mn^{2+} and Mn^{4+} (Luther 2005). If it is produced, Mn^{3+} can only persist if it is stabilized as a mineral or chelated by ligands; otherwise, it is rapidly oxidized to Mn^{4+} or reduced to Mn^{2+} (Madden and Hochella 2005; Webb 2005; Lan et al. 2017).1/7/2026 11:16:00 PM Accordingly, the most efficient litter-degrading fungi, the white-rot fungi, produce a Mn-dependent enzyme (Mn peroxidases) to overcome the thermodynamic challenges Mn^{3+} poses and take advantage of its potency: Mn peroxidase oxidizes Mn^{2+} to Mn^{3+} to attack and degrade OM by depolymerizing complex molecular constituents of OM, especially lignin (Hofrichter 2002). Thermodynamics underlies why Mn peroxidase is the likely reason that decomposing litter accumulates oxidized Mn in the form of $Mn^{3+/4+}$-oxides (Berg et al. 2010; Keiluweit et al. 2015).

Plants take up Mn^{2+} from the rhizosphere through root cells, releasing H^+ or low-molecular-weight organic acids to acidify the local environment and reduce Mn-oxides into bioavailable Mn (Rengel and Marschner 2005). In general, acidic and/or reducing soil conditions favor Mn uptake in plants; basic and/or oxidizing soil conditions diminish Mn availability. Once absorbed, Mn is quickly transported through the xylem to photosynthetically active leaves via the transpiration

59 stream (Page and Feller 2005). Consequently, Mn accumulates mostly in leaves but, due to its
60 diverse biological roles, is found throughout the plant, mostly as Mn^{2+} (Alejandro et al. 2020).
61 Plants do not resorb Mn during leaf senescence; as their leaves die and fall to the ground, they
62 return Mn to surface soils, where decomposition oxidizes Mn^{2+} in litter to $Mn^{3+/4+}$-oxides (Herndon
63 et al. 2015; Keiluweit et al. 2015)

64 Despite the tight recycling of plant-litter Mn, plants can absorb Mn at 100–1000 times the
65 rate at which they use the nutrient (Clarkson 1988); some species' absorption rates mirror Mn^{2+}
66 concentrations in soils, even to toxic levels (Marschner 1988; Fernando and Lynch 2015).
67 Differences in species' sensitivities to Mn toxicity is posited to have reshaped a temperate
68 grassland that was treated with nitrogen (N) for a decade—N amendments acidified the soil, which
69 increased Mn bioavailability to toxic levels and transformed the once forb- and grass-dominated
70 community to exclusively grasses (forbs are more sensitive to Mn toxicity) (Tian et al. 2016);
71 moreover, greater N additions correlated with greater Mn liberation and increased litter
72 decomposition rates (Hou et al. 2021). Such shifts in litter biomass and decomposition rates
73 suggest that Mn may shape an ecosystem's C cycle. However, how Mn does so remains unclear,
74 especially in grasslands, a largely overlooked ecosystem in Mn studies.

75 Grasslands cover approximately one-quarter of Earth's land surface, account for roughly
76 one-third of net primary production on land, and store around 12% of total terrestrial C (Hoekstra
77 et al. 2005; Janowiak et al. 2017). Their productivity makes them exceptionally useful to humans
78 for food and forage production, and vulnerable to degradation and consequent C loss: 20–25% of
79 grasslands have been degraded (Janowiak et al. 2017). We need to know how vulnerable or
80 resilient grassland C stocks are to Mn redox cycles.

OM stability depends on the ecosystem, hinging on complex interactions among the abiotic and biotic factors of an environment (Schmidt et al. 2011; Lehmann and Kleber 2015). An ecosystem's climate, potential organo-mineral interactions, nutrient accessibility, and plant and microbial community and functioning influence OM decomposition. Accordingly, Mn may not exercise the same control on litter decomposition in a grassland as it reportedly does in forests (Fujii et al. 2020; Santos and Herndon 2023). And the effect of foliar Mn versus soil-derived Mn on litter decomposition is poorly known. We use field and laboratory experiments to evaluate these dynamics on the Kohala rainfall gradient in areas with different foliar and soil Mn abundances, and on which a single plant species (kikuyu [*Pennisetum clandestinum*]) dominates primary production and the litter pool.

2. Materials and Methods

2.1. Gradient Sites

Samples were decomposed in and collected from three sites on the Kohala Mountain rainfall gradient, a ~14-km transect on the Island of Hawai'i that receives from <300 to >3200 mm mean annual precipitation (MAP) (Giambelluca et al. 2013); mean annual temperatures and elevation range from 23.5 °C and 50 m at the dry end to 16 °C and 1000 m at the wet end (Giambelluca et al. 2014). Although temperature, elevation, and rainfall vary along the Kohala gradient, previous studies on the gradient suggest that rainfall (and water availability) primarily underlie the emergent shifts in pedology and ecology (Chadwick et al. 2003; von Sperber et al. 2017; Vitousek et al. 2021).

Three experimental sites that receive ~1578, 2163, or 3238 mm MAP were chosen because all three points are Andisols located on the same ~150,000-year-old Hawī volcanic formation

(Chadwick et al. 2003; Sherrod et al. 2007), possess the same relief, are moderately acidic (Table 1), and have been grazed by cattle for over 100 years (Kagawa and Vitousek 2012). Field sites' approximate locations are shown in Fig. S1. In all three sites, a single species of kikuyu grass (*Pennisetum clandestinum)* dominates primary production and (consequently) the litter pool; soil nutrients are relatively abundant here (Chadwick et al. 2007; Vitousek and Chadwick 2013), Basidiomycota DNA (the fungal group that includes ligninolytic white rot fungi) have been identified (Peay et al. 2017), and Mn peroxidase activity has been detected on this gradient (Paulus and Vitousek 2024). Each site also possesses distinct concentrations of Mn in its soil and in kikuyu grass (Table 1, Fig. S2): of these three sites, the driest site has the greatest soil and lowest grass Mn concentrations, the middle MAP site has moderate soil and the greatest grass Mn concentrations, and the wettest site has the lowest soil and moderate plant Mn concentrations.

2.2. Soil and Litter Collection

Soil and grass samples were collected in the summers of 2018 and/or 2019 and were measured in at least triplicate (n = 3–6). Soil samples were collected as continuous 10-cm cores from the A horizon, sealed in two layers of plastic bags, manually homogenized to remove root matter and rocks, and frozen at -20°C. To determine percent soil moisture, subsamples were sieved to 2 mm, weighed, and oven-dried at 65˚C to constant weight. Grass collection was limited to aboveground litter. For chemical analyses, grass litter subsamples were oven-dried at 65°C and ground using a Wiley Mill. We determined background Mn concentrations in dried, ground soil and litter subsamples using X-ray fluorescence (XRF); background Mn data are presented in Fig. S2.

In August 2021, freshly senesced kikuyu leaves were collected from the three of the gradient sites for the field and laboratory decomposition experiments. The leaf litter was air dried,

127 weighed, and separated into ~1g aliquots. Each aliquot was sewn into a mesh litter bag (Fig. S3)
128 and reweighed. Litter bags were constructed from 6cm x 12cm sections of 0.011-gauge fiberglass
129 insect screen cloth folded in half lengthwise and secured by ribbon sewn onto three sides of the
130 resulting $6cm^2$ square.
131
132 *2.3. Litter-decomposition Field Experiment*
133 The field experiment was designed to parse the relative contributions of foliar versus soil Mn to
134 litter decomposition under different rainfall regimes. Kikuyu dominates the plant communities,
135 primary production, and the litter pools in all three sites (1578, 2163, and 3238 mm MAP). We
136 collected grass litter at each site, created grass litter bags, and distributed the litter bags among the
137 three sites: three bags from each site were left to decompose at all sites for 5 or 12 months. Three
138 additional bags per site were immediately preserved at 4°C for initial chemical and synchrotron
139 analyses. At the end of the 5- and 12-month decompositions, at least three bags of each type were
140 collected from each decomposition site and preserved at 4°C for 5- and 12-month-group analyses.
141 We assessed mass loss, C content, Mn concentration, and distributions of Mn oxidation states in
142 each litter bag to evaluate whether Mn concentration and availability correlate with litter
143 decomposition and, if so, whether foliar or soil Mn better predicts the extent of litter
144 decomposition.
145
146 *2.4. Manganese-treatment Incubation Experiment*
147 In addition to the field experiment, we used a laboratory decomposition experiment to directly test
148 the effects of Mn abundance and availability on litter decomposition. We collected kikuyu litter
149 from three gradient sites (receiving 1578, 2163, or 3238 mm MAP), air dried the litter, and divided

the litter into ~1 g aliquots per litter bag. We also subsampled litter for background/initial chemical analyses. To serve as substrate for the incubation, soil containing low background Mn (~644 µg Mn/g dried soil; Table 1) was collected from the wettest site. Three litter bags from each site were randomly assigned to one of two conditions: control or Mn treatment. Both conditions were maintained at 25°C on a laboratory bench in equivalent un-lidded plastic tubs.

For ten months, the control and Mn-treatment conditions received weekly additions of 495 ml of deionized (DI) water (no additional Mn) or 17.6-µM manganese chloride ($MnCl_2$), respectively, to approximate the average daily rainfall of the wettest site. These additions were dispersed uniformly across the soil substrate (and incubation container's floor) (Fig. S3). Over the ten-month incubation, the Mn treatments provided ~2 mg total of supplemental Mn per g initial dry litter mass (0.35 g Mn m^{-2}). At the end of the experiment, we harvested the litter to assess mass loss, changes in C and Mn contents, and distributions of Mn oxidation states across litter surfaces.

2.5. Laboratory Analyses

Grass litter was air dried and weighed before and after decomposing to assess mass loss; initial samples of each experimental type were air dried and weighed immediately following collection. Subsets of each litter type were oven dried at 65°C to constant weight to characterize air-dry-to-oven-dry mass conversions and for C content and total Mn analyses; C content was determined using a Carlo Erba NA 1500 Elemental Analyzer (EA), and Mn concentration was measured using inductively coupled plasma optical emission spectroscopy (ICP-OES), performed on a Thermo-Fisher ICAP 6300 Duo View. To measure soil pH, soil samples were mixed with DI water in 1g:1mL slurries and shaken for 5 min (Thomas 1996); slurries stood for 10 min before pH was read. Each soil pH is reported as an average of six measurements (Table 1). EA, ICP-OES. EA,

ICP-OES, and XRF measurements were performed in the Environmental Measurements Facility (EMF) at Stanford University.

2.6. Micro-X-ray Absorption Spectroscopy Imaging

Mn distribution and oxidation states on grass litter were determined using elemental maps and Mn micro-X-ray absorption near edge structure (μXANES) spectra. Samples were stored at -20°C between collection and synchrotron imaging. Micro-X-ray absorption spectroscopy (μXAS) imaging was performed on beamline 7–2 at the Stanford Synchrotron Radiation Lightsource (SSRL), SLAC National Accelerator Laboratory. This beamline uses a water-cooled, double-crystal Si(111) monochromator; the energy was calibrated using the first derivative of a Mn metal foil to 6537.7 eV (Manceau et al. 2012). Litter samples were sealed into sample holders using X-ray-transparent Kapton tape and polyethylene plastic wrap.

Each litter sample was initially imaged using coarse resolution to map total Mn abundance. We used these data to choose regions for Mn multi-energy mapping and X-ray absorption near edge structure (XANES) spectroscopy to map Mn oxidation states across litter surfaces. Fine-resolution images were generated using a 25μm beam focus on small areas of interest. We used principal component analyses (PCA) and simplex volume maximization (SiVM) in SMAK (v2.00) to choose the most appropriate locations for XANES spectroscopy (Webb 2011; Alfeld et al. 2017; Kravchenko et al. 2022). XANES spectra were normalized and verified in SixPack (v1.5.6) using previously published standards (Hansel et al. 2012; Johnson et al. 2016).

To compare relative densities of Mn oxidation states on litter surfaces, we used SMAK to perform particle statistics and particle-density analyses. Particles were distinguished from backgrounds using InvBinary or Otsu thresholding algorithms, and the minimum-sized particle

was defined as two pixels. Particle-density analyses identified particles in sample images as Mn^{2+}, Mn^{3+}, or Mn^{4+} following PCA and XANES analyses. Regions of Interest (ROI) were assigned by the Particle Statistics function in SMAK.

2.7. Statistical and Data Analyses

Means and standard errors of means were calculated for all soil analyses. We applied the Shapiro-Wilk test to assess normality in all datasets. When the data satisfied normality assumptions, we applied parametric tests: One Way Analysis of Variance (ANOVA), Two Way ANOVA, and Tukey's Honest Significant Difference (HSD) post-hoc test, or the Student's T-test. When the data did not meet normality assumptions, we applied nonparametric tests: the Kruskal-Wallis test and the Dunn-Bonferroni post-hoc test or the Wilcoxon-Mann-Whitney test. Significance was determined as p-values ≤ 0.05. Calculations, graphing, and statistics were performed in Microsoft Excel (v16.67) and R (v4.2.2). Synchrotron data were collected using SMAK (v2.00) (Webb 2011); spectra normalizations and statistics (Principal Component Analyses [PCA] and Linear Combination Fitting [LCF]) were performed using Sixpack (v1.5.6) (Webb 2005). Kohala gradient mean annual precipitations (MAP) were reported from Giambelluca et al. 2013.

3. Results

3.1. Field Litter-decomposition Experiment

To assess how litter Mn concentrations changed with decomposition, we compared Mn concentrations in initial and 5-month-decomposed litter collected from all three sites (Fig. 1A). The litter was too degraded and sparse to determine Mn concentrations in the samples that were decomposed in Site 3 for 5 months and in all sites for 12 months. Initial litter Mn concentrations

generally increased with rainfall: the Mn concentration in litter collected from the driest site (L1) was significantly lower than at the wettest site's (L3); litter collected from the moderate rainfall site (L2) did not significantly differ from the other two sites. After 5 months, the greatest Mn concentrations were found in litter decomposed in Site 1, with L1 and L3 showing significantly greater Mn concentrations than their counterparts decomposed in Site 2. L1 decomposed in Site 1 showed the greatest Mn concentrations of any group, initial or decomposed. Mn concentrations in litter decomposed in Site 2 did not significantly differ across litter types (L1, L2, and L3).

μXRF imaging analyses reveal Mn compositions on the surface of litter shifted over 12-month decompositions (Fig. 1B); the μXRF images sourced for the particle-density analyses are shown in Fig. S4. Litter collected from Site 1 (L1) initially showed Mn^{2+} and Mn^{4+} on its surface. After 12 months, Mn^{2+} disappeared from the surfaces of L1 litter decomposed in sites 1 and 2, while Mn^{+3} appeared with Mn^{4+}; litter decomposed in Site 3 did not differ in Mn composition from the initial litter. Litter collected from Site 2 (L2) also initially presented Mn^{2+} and Mn^{4+} on its surface. Mn^{4+} was the only oxidation state apparent on L2 litter decomposed in sites 1 and 2, while all three oxidation states appeared in the litter decomposed in Site 3. Lastly, L3 litter initially presented almost exclusively Mn^{4+} and little Mn^{2+}. Decomposed L3 litter showed Mn^{4+} dominated Mn compositions in litter decomposed in all three sites: Mn^{3+} contributed little to Mn compositions in litter decomposed in sites 1 and 2, and Mn^{2+} was absent in decomposed litter from all sites.

We measured mass loss in all litter types to indicate degree of decomposition. After 5 months, litter types decomposed in Site 3 generally showed the greatest mass loss (Fig. 1C); this relationship was statistically strongest for L2. Litter decomposed in Site 1 and 2 did not significantly differ in mass loss. 12-month decompositions show no consistent pattern (Fig. 1D).

241 Linear analyses between 5-month-decomposition mass loss and litter Mn, soil Mn, and
242 MAP reveal the only positive association between mass loss and MAP (Fig. 2); litter Mn and soil
243 Mn showed negative linear relationships. The difference between R^2 values for 5-month- and 12-
244 month-decompostion % mass loss versus MAP (0.63 and 0.09, Fig. 2E, F) confirms that MAP
245 reliably predicts % mass loss for the 5-month decomposition but not for the 12-month
246 decomposition. Accordingly, MAP and not Mn (whether foliar or soil) correlates with litter
247 decomposition in the field.

248 We evaluated carbon-to-nitrogen ratios (C/N) as another metric of litter decomposition
249 over 5 months and 12 months (Fig. S5); decreased C/N in litter generally indicates greater
250 decomposition. We found no statistically significant differences among the permutations of litter
251 type and decomposition site for either the 5-month or 12-month field experiment.

252

253 *3.2. Manganese-treatment Incubation Experiment*

254 Particle density analyses of litter from the incubation experiment reveal distinct patterns in Mn
255 oxidation states on litter surfaces (Fig. 3); source μXAS images of litter are shown in Fig. S6. Mn
256 treatment significantly increased Mn^{2+} in the Mn-treated litter from Site 2 but no other site (Fig.
257 3A, D); Mn^{3+} and Mn^{4+} prevalence did not change with Mn treatment (Fig. 3B, C, D). To isolate
258 the effect of Mn availability on litter Mn oxidation states, we compared the aggregated control
259 versus Mn treatment data (Fig. 3E, F). Paired analyses revealed that Mn treatment significantly
260 increased the percentages of Mn^{2+} and Mn^{3+} but not Mn^{4+} on decomposed litter (Fig. 3E). These
261 data confirm that Mn treatment increased Mn bioavailability at the surface but not necessarily Mn
262 redox cycling.

263 Whether analyzed according to litter type or aggregate condition, no significant differences
264 were found in mass loss between the control and Mn treatment groups (Fig. 4A, B). Similarly, no
265 differences in C/N ratios were found between the control and Mn treatment groups, whether
266 divided by litter type or examined in aggregate (Fig. S7A, B). Accordingly, Mn treatment
267 (increased Mn abundance and availability) did not increase litter decomposition over the 10-month
268 laboratory incubation experiment.
269
270 **4. Discussion**
271 We hypothesized that Mn bioavailability would correlate with litter decomposition in the field and
272 laboratory experiments. While a 6-year decomposition time was used for pine needles in a
273 temperate forest (Keiluweit et al. 2015), we used shorter study periods (5, 10, and 12 months)
274 because we expected to see rapid litter decomposition in the Kohala grassland due to the sites'
275 nutrient availability (Chadwick et al. 2007; Schmidt et al. 2011; Vitousek and Chadwick 2013;
276 Lehmann and Kleber 2015), the activity of the ligninolytic enzyme Mn peroxidase in the sites
277 (Paulus and Vitousek 2024), and grass's low lignin content (relative to pine needles')
278 (Meentemeyer 1978; Melillo et al. 1982; Wedin and Tilman 1990; Talbot et al. 2012; Santos and
279 Herndon 2023). We observed differences in Mn content and shifts in Mn oxidation states on litter
280 as it decomposed in the field and laboratory, suggesting Mn could mechanistically degrade litter;
281 but we found no evidence that Mn governed litter decomposition.
282 In the field experiment, Mn accumulated in all litter that decomposed for 5 months in Site
283 1 relative to freshly senesced litter collected along the gradient (Fig. 1A); Mn content did not
284 change in litter decomposed in Site 2, and there was not enough material to measure Mn in grass
285 decomposed in Site 3. μXAS analyses of litter surfaces demonstrated that the composition of Mn

oxidation states evolved from Mn^{2+} and Mn^{4+} on freshly senesced grass leaves to Mn^{2+}, Mn^{3+}, and Mn^{4+} on 12-month-decomposed litter (Fig. 1B; Fig. S4). Mn^{2+} and Mn^{3+} mark the early stages of decomposition; as decomposition progresses, Mn oxidizes into $Mn^{3+/4+}$, especially in hotspots of OM breakdown (Thompson et al. 2005; Hansel et al. 2012; Herndon et al. 2014; Keiluweit et al. 2015). We expected the greater Mn concentration and oxidation to correlate with greater litter decomposition, evidenced by increased mass loss and decreased C/N ratios. However, mass loss correlated with MAP (Fig. 2), not with Mn content, and there were no significant differences among C/N ratios among the litter types decomposed for 5 or 12 months (Fig. S5).

Despite controlling for water availability and temperature, similar patterns emerge from the laboratory incubation study. Over the ten-month incubation, the Mn treatments provided a total of ~2 mg of available supplemental Mn per g initial dry litter mass. This concentration of supplementary Mn was three times the substrate soil's Mn concentration and 7–29 times the grass litters' Mn concentrations (Table 1). This additional Mn was sufficient to observe the effect of supplementary Mn availability without risking Mn toxicity to the fungal community decomposing the litter: Mn treatment successfully supplemented the availability of Mn^{2+}, which translated to greater total Mn^{3+} in the Mn treatment group in comparison to the control (Fig. 3E; Fig. S6); fungal hyphae were also visible in Mn treated litter bags and not in control litter bags (Fig. S3). The primary mechanism through which Mn is posited to degrade litter is through the ligninolytic enzyme Mn peroxidase. Given that lignin generally composes 5% of grassland litter versus 19% of temperate forest litter, our Mn application was comparable on a per g lignin basis to previous studies that investigated the effect of Mn on temperate forests' litter decay (Meentemeyer 1978; Melillo et al. 1982; Wedin and Tilman 1990; Gholz et al. 2000; Whalen et al. 2018; Zhang et al. 2024). But these differences in Mn content, Mn oxidation states, and apparent fungal activity did

not correspond with greater mass loss (Fig. 4) or decreased C/N ratios (Fig. S7) in the Mn-treated litter. We did not see Mn treatment enhance litter decomposition over the 10-month decomposition experiment.

Although, in the current study, we saw evidence of Mn oxidation and fungal activity (Fig. S6 and Fig. S3C–F)—the primary mechanism through which Mn may destabilize organic matter—and previous studies discovered evidence of Basidiomycota and Mn peroxidase activity in the experimental sites (Peay et al. 2017; Paulus and Vitousek 2024), we found no correlation between Mn content (foliar, soil, or total) and grass litter decomposition. Even when water availability and temperature (proxies for MAP in the field study) were controlled in the incubation experiment, Mn abundance and availability did not determine litter decay. Previous studies that observed links between Mn and litter loss focused on spruce and needle litter from temperate forests, following their decay over longer experimental periods than in the present study (Berg 2000; Davey et al. 2007; Keiluweit et al. 2015; Berg et al. 2015). Whaley et al. 2018 also studied needle litter under Mn amendment but limited their experiment to 6 months; as in our study, they found Mn addition did not increase total litter mass loss. The authors note that their study could have been too short, proposing that Mn amendments would have increased litter mass loss during late-stage decay rather than early-stage because the relationship between Mn and litter decay strengthens as litter decay proceeds (Berg et al. 2007).

It is unlikely, however, that our experiments were too short to observe Mn influence decay. In the field study, most litter bags lost ≥ 50% mass. So little litter remained in the litter bags after 12 months that it was difficult to distinguish grass litter from incidental matter that might have washed through the screen with rainfall and remained caught in the bag; this was especially true of the litter bags that decomposed in Site 3 (the wettest site). The laboratory study litter bags saw

comparable mass losses of ~50%. Furthermore, the shifts in Mn oxidation states, from reduced to oxidized, suggests the litter samples experienced advanced stages of breakdown. The litter decayed, but not as predicted by Mn availability and oxidation state. Accordingly, Mn does not control grass litter decomposition in this ecosystem.

While Mn availability may be the "single main factor" predicting litter decomposition in temperate forests (Berg et al. 2010), it does not appear to wield the same influence in grasslands—despite evidence of Mn peroxidase and fungal activity in the incubation and field experiments. Why Mn has distinct influences in grasslands and forests is not clear. In forest soils, Mn peroxidase appears to perform most efficiently around pH 4.5–5 (Fujii et al. 2013, 2020). The Kohala sites' soil pH range from 4.1520–5.328 (Table 1); this evidence and the Mn peroxidase activity measured in these sites suggests that the Mn peroxidase produced here should be viable. But perhaps the Basidiomycetes in these sites do not produce enough of this enzyme (within the suite of decomposition enzymes they produce) for Mn to determine decomposition rate. Further study on Mn-dependent enzyme activity and expression is warranted in grasslands to investigate if these findings apply broadly to grasslands.

In forests, foliar Mn concentration increases with lignin content and decomposition rate, and high Mn/lignin ratios correlate with greater Mn peroxidase activities (Fujii et al. 2020; Santos and Herndon 2023). Grass litter contains less lignin than forest litter (*e.g.*, pine needles) does, perhaps indicating one reason why Mn does not predict litter decay in the grassland as it seems to in forests. The distinct substrate chemistries in grasslands versus forests do not alone explain the difference; they reflect their ecosystems' distinct environments and microbial-community functioning that regulates decomposition (Schmidt et al. 2011; Lehmann and Kleber 2015). Future

studies should more deeply interrogate these microbial communities, their activities, and the environmental factors (*e.g.*, redox conditions) that shape both.

Mn availability and oxidation state did not predict grass litter decomposition—either along a grassland rainfall gradient under field conditions or in Mn-treated incubations. These findings suggest that Mn is cycling in the grassland at capacity—the ecosystem's microbial-community composition and/or resource availability cannot support faster or greater Mn cycling, rendering supplemental Mn inconsequential to litter decomposition. The importance of Mn to an ecosystem's C cycle may only emerge as other environmental factors converge to otherwise retard the rate of decay.

5. Acknowledgements

We thank Parker Ranch, Ponoholo Ranch, and Kamehameha Schools for access to the research sites; Ulu Mau Puanui for equipment support; Kehaulani Marshall and Healohamele Genovia for field assistance; Doug Turner and Dr. Guangchao Li for laboratory analyses; Drs. Juan Lezama, Kristin Boye, and Sam Webb for SLAC SSRL synchrotron data collection and interpretation; and Drs. Scott Fendorf, Oliver Chadwick, Karen Casciotti, and Kabir Peay of Stanford University for their invaluable input on this work.

6. Declarations

Funding: This work was supported by United States National Science Foundation Award Number 2027290, in collaboration with Dr. Mengqiang Zhu (University of Wyoming). ELP was also supported by the Department of Energy Science Graduate Student Research Fellowship (DOE SCGSR).

Conflicts of interest/Competing interests: The authors declare that they have no conflict of interest nor competing interests.

Ethics approval: NA

Consent to participate: NA

Consent for publication: NA

Availability of data and material: The datasets used and/or analyzed during the current study are available from the corresponding author on reasonable request.

Code availability: The code used during the current study are available from the corresponding author on reasonable request.

Author contributions: ELP and PMV designed the study and conducted the fieldwork. ELP conducted the laboratory analyses, analyzed the data, and wrote the article with contributions from PMV.

7. References

Alejandro S, Höller S, Meier B, Peiter E (2020) Manganese in plants: From acquisition to subcellular allocation. Front Plant Sci 11:300. https://doi.org/10.3389/fpls.2020.00300

Alfeld M, Wahabzada M, Bauckhage C, et al (2017) Simplex volume maximization (SiVM): A matrix factorization algorithm with non-negative constrains and low computing demands for the interpretation of full spectral X-ray fluorescence imaging data. Microchemical Journal 132:179–184. https://doi.org/10.1016/j.microc.2017.02.001

Berg B (2000) Litter decomposition and organic matter turnover in northern forest soils. Forest Ecology and Management 133:13–22. https://doi.org/10.1016/S0378-1127(99)00294-7

Berg B, Davey MP, De Marco A, et al (2010) Factors influencing limit values for pine needle litter decomposition: a synthesis for boreal and temperate pine forest systems. Biogeochemistry 100:57–73. https://doi.org/10.1007/s10533-009-9404-y

Berg B, Erhagen B, Johansson M-B, et al (2015) Manganese in the litter fall-forest floor continuum of boreal and temperate pine and spruce forest ecosystems – A review. Forest Ecology and Management 358:248–260. https://doi.org/10.1016/j.foreco.2015.09.021

405 Berg B, McClaugherty C (2003) Plant litter. Springer Berlin Heidelberg, Berlin, Heidelberg

406 Berg B, Steffen KT, McClaugherty C (2007) Litter decomposition rate is dependent on litter Mn
407 concentrations. Biogeochemistry 82:29–39. https://doi.org/10.1007/s10533-006-9050-6

408 Chadwick OA, Gavenda RT, Kelly EF, et al (2003) The impact of climate on the biogeochemical
409 functioning of volcanic soils. Chemical Geology 202:195–223.
410 https://doi.org/10.1016/j.chemgeo.2002.09.001

411 Chadwick OA, Kelly EF, Hotchkiss SC, Vitousek PM (2007) Precontact vegetation and soil
412 nutrient status in the shadow of Kohala Volcano, Hawaii. Geomorphology 89:70–83.
413 https://doi.org/10.1016/j.geomorph.2006.07.023

414 Clarkson DT (1988) The uptake and translocation of manganese by plant roots. In: Graham RD,
415 Hannam RJ, Uren NC (eds) Manganese in Soils and Plants. Springer Netherlands,
416 Dordrecht, pp 101–111

417 Cui F, Dolphin D (1990) The role of manganese in model systems related to lignin
418 biodegradation. Holzforschung 44:279–283. https://doi.org/10.1515/hfsg.1990.44.4.279

419 Davey MP, Berg B, Emmett BA, Rowland P (2007) Decomposition of oak leaf litter is related to
420 initial litter Mn concentrations. Can J Bot 85:16–24. https://doi.org/10.1139/b06-150

421 Fernando DR, Lynch JP (2015) Manganese phytotoxicity: new light on an old problem. Ann Bot
422 116:313–319. https://doi.org/10.1093/aob/mcv111

423 Fujii K, Nakada Y, Umezawa K, et al (2020) A comparison of lignin-degrading enzyme
424 activities in forest floor layers across a global climatic gradient. Soil Ecol Lett 2:281–
425 294. https://doi.org/10.1007/s42832-020-0042-6

426 Fujii K, Uemura M, Hayakawa C, et al (2013) Environmental control of lignin peroxidase,
427 manganese peroxidase, and laccase activities in forest floor layers in humid Asia. Soil
428 Biology and Biochemistry 57:109–115. https://doi.org/10.1016/j.soilbio.2012.07.007

429 Gholz HL, Wedin DA, Smitherman SM, et al (2000) Long-term dynamics of pine and hardwood
430 litter in contrasting environments: toward a global model of decomposition. Global
431 Change Biology 6:751–765. https://doi.org/10.1046/j.1365-2486.2000.00349.x

432 Giambelluca TW, Chen Q, Frazier AG, et al (2013) Online rainfall atlas of Hawai‘i. Bulletin of
433 the American Meteorological Society 94:313–316. https://doi.org/10.1175/BAMS-D-11-
434 00228.1

435 Giambelluca TW, Shuai X, Barnes M, et al (2014) Evapotranspiration of Hawai’i: Final report.
436 US Army Corps of Engineers, Honolulu District, and the Commission on Water Resource
437 Management, State of Hawai’i

438 Hansel CM, Zeiner CA, Santelli CM, Webb SM (2012) Mn(II) oxidation by an ascomycete
439 fungus is linked to superoxide production during asexual reproduction. Proceedings of

440 the National Academy of Sciences of the United States of America 109:12621–12625.
441 https://doi.org/10.1073/pnas.1203885109

442 Herndon EM, Jin L, Andrews DM, et al (2015) Importance of vegetation for manganese cycling
443 in temperate forested watersheds: Biogeochemistry of Mn contaminants. Global
444 Biogeochem Cycles 29:160–174. https://doi.org/10.1002/2014GB004858

445 Herndon EM, Martínez CE, Brantley SL (2014) Spectroscopic (XANES/XRF) characterization
446 of contaminant manganese cycling in a temperate watershed. Biogeochemistry 121:505–
447 517. https://doi.org/10.1007/s10533-014-0018-7

448 Hoekstra JM, Boucher TM, Ricketts TH, Roberts C (2005) Confronting a biome crisis: global
449 disparities of habitat loss and protection. Ecology Letters 8:23–29.
450 https://doi.org/10.1111/j.1461-0248.2004.00686.x

451 Hofrichter M (2002) Review: lignin conversion by manganese peroxidase (MnP). Enzyme and
452 Microbial Technology 30:454–466. https://doi.org/10.1016/S0141-0229(01)00528-2

453 Hou S-L, Hättenschwiler S, Yang J-J, et al (2021) Increasing rates of long-term nitrogen
454 deposition consistently increased litter decomposition in a semi-arid grassland. New
455 Phytologist 229:296–307. https://doi.org/10.1111/nph.16854

456 Janowiak M, Connelly WJ, Dante-Wood K, et al (2017) Considering forest and grassland carbon
457 in land management. U.S. Department of Agriculture, Forest Service, Washington Office,
458 Washington, DC

459 Johnson JE, Webb SM, Ma C, Fischer WW (2016) Manganese mineralogy and diagenesis in the
460 sedimentary rock record. Geochimica et Cosmochimica Acta 173:210–231.
461 https://doi.org/10.1016/j.gca.2015.10.027

462 Jones ME, Nico PS, Ying S, et al (2018) Manganese-driven carbon oxidation at oxic–anoxic
463 interfaces. Environ Sci Technol 52:12349–12357.
464 https://doi.org/10.1021/acs.est.8b03791

465 Kagawa AK, Vitousek PM (2012) The ahupua‘a of Puanui: A resource for understanding
466 Hawaiian rain-fed agriculture. Pacific Science 66:161–172. https://doi.org/10.2984/66.2.6

467 Keiluweit M, Nico P, Harmon ME, et al (2015) Long-term litter decomposition controlled by
468 manganese redox cycling. Proceedings of the National Academy of Sciences 112:E5253–
469 E5260. https://doi.org/10.1073/pnas.1508945112

470 Keiluweit M, Nico PS, Kleber M, Fendorf S (2016) Are oxygen limitations under recognized
471 regulators of organic carbon turnover in upland soils? Biogeochemistry 127:157–171.
472 https://doi.org/10.1007/s10533-015-0180-6

473 Kravchenko AN, Richardson JA, Lee JH, Guber AK (2022) Distribution of Mn oxidation states
474 in grassland soils and their relationships with soil pores. Environ Sci Technol 56:16462–
475 16472. https://doi.org/10.1021/acs.est.2c05403

476 Lan S, Wang X, Xiang Q, et al (2017) Mechanisms of Mn(II) catalytic oxidation on ferrihydrite
477 surfaces and the formation of manganese (oxyhydr)oxides. Geochimica et Cosmochimica
478 Acta 211:79–96. https://doi.org/10.1016/j.gca.2017.04.044

479 Lehmann J, Kleber M (2015) The contentious nature of soil organic matter. Nature 528:60–68.
480 https://doi.org/10.1038/nature16069

481 Luther GW (2005) Manganese(II) oxidation and Mn(IV) reduction in the rnvironment—Two
482 one-electron transfer steps versus a single two-electron step. Geomicrobiology 22:195–
483 203. https://doi.org/10.1080/01490450590946022

484 Madden AS, Hochella MF (2005) A test of geochemical reactivity as a function of mineral size:
485 Manganese oxidation promoted by hematite nanoparticles. Geochimica et Cosmochimica
486 Acta 69:389–398. https://doi.org/10.1016/j.gca.2004.06.035

487 Manceau A, Marcus MA, Grangeon S (2012) Determination of Mn valence states in mixed-
488 valent manganates by XANES spectroscopy. American Mineralogist 97:816–827.
489 https://doi.org/10.2138/am.2012.3903

490 Marschner H (1988) Mechanisms of manganese acquisition by roots from soils. In: Graham RD,
491 Hannam RJ, Uren NC (eds) Manganese in Soils and Plants: Proceedings of the
492 International Symposium on 'Manganese in Soils and Plants' held at the Waite
493 Agricultural Research Institute, The University of Adelaide, Glen Osmond, South
494 Australia, August 22–26, 1988 as an Australian Bicentennial Event. Springer
495 Netherlands, Dordrecht, pp 191–204

496 Meentemeyer V (1978) Macroclimate and lignin control of litter decomposition rates. Ecology
497 59:465–472. https://doi.org/10.2307/1936576

498 Melillo JM, Aber JD, Muratore JF (1982) Nitrogen and lignin control of hardwood leaf litter
499 decomposition dynamics. Ecology 63:621–626. https://doi.org/10.2307/1936780

500 Page V, Feller U (2005) Selective Transport of zinc, manganese, nickel, cobalt and cadmium in
501 the root system and transfer to the leaves in young wheat plants. Ann Bot 96:425–434.
502 https://doi.org/10.1093/aob/mci189

503 Paulus EL, Vitousek PM (2024) Manganese and soil organic carbon stability on a Hawaiian
504 grassland rainfall gradient. Soil Biology and Biochemistry 194:109418.
505 https://doi.org/10.1016/j.soilbio.2024.109418

506 Peay KG, von Sperber C, Cardarelli E, et al (2017) Convergence and contrast in the community
507 structure of Bacteria, Fungi and Archaea along a tropical elevation–climate gradient.
508 FEMS Microbiology Ecology 93:fix045. https://doi.org/10.1093/femsec/fix045

509 Rengel Z, Marschner P (2005) Nutrient availability and management in the rhizosphere:
510 exploiting genotypic differences. New Phytologist 168:305–312.
511 https://doi.org/10.1111/j.1469-8137.2005.01558.x

512 Rezanezhad F, Couture R-M, Kovac R, et al (2014) Water table fluctuations and soil
513 biogeochemistry: An experimental approach using an automated soil column system.
514 Journal of Hydrology 509:245–256. https://doi.org/10.1016/j.jhydrol.2013.11.036

515 Santos F, Herndon E (2023) Plant-soil relationships influence observed trends between
516 manganese and carbon across biomes. Global Biogeochemical Cycles
517 37:e2022GB007412. https://doi.org/10.1029/2022GB007412

518 Schmidt MWI, Torn MS, Abiven S, et al (2011) Persistence of soil organic matter as an
519 ecosystem property. Nature 478:49–56. https://doi.org/10.1038/nature10386

520 Sherrod DR, Sinton JM, Watkins SE, Brunt KM (2007) Geologic map of the State of Hawai‘i. 85

521 Talbot JM, Yelle DJ, Nowick J, Treseder KK (2012) Litter decay rates are determined by lignin
522 chemistry. Biogeochemistry 108:279–295. https://doi.org/10.1007/s10533-011-9599-6

523 Thomas GW (1996) Soil pH and soil acidity. In: Methods of Soil Analysis. John Wiley & Sons,
524 Ltd, pp 475–490

525 Thompson IA, Huber DM, Guest CA, Schulze DG (2005) Fungal manganese oxidation in a
526 reduced soil. Environ Microbiol 7:1480–1487. https://doi.org/10.1111/j.1462-
527 2920.2005.00842.x

528 Tian Q, Liu N, Bai W, et al (2016) A novel soil manganese mechanism drives plant species loss
529 with increased nitrogen deposition in a temperate steppe. Ecology 97:65–74.
530 https://doi.org/10.1890/15-0917.1

531 van der Lee G (1999) Anoxic microsites in Douglas fir litter. Soil Biology and Biochemistry
532 31:1295–1301. https://doi.org/10.1016/S0038-0717(99)00048-6

533 Vitousek PM, Bateman JB, Chadwick OA (2021) A “toy” model of biogeochemical dynamics on
534 climate gradients. Biogeochemistry 154:183–210. https://doi.org/10.1007/s10533-020-
535 00734-y

536 Vitousek PM, Chadwick OA (2013) Pedogenic thresholds and soil process domains in basalt-
537 derived soils. Ecosystems 16:1379–1395. https://doi.org/10.1007/s10021-013-9690-z

538 von Sperber C, Chadwick OA, Casciotti KL, et al (2017) Controls of nitrogen cycling evaluated
539 along a well-characterized climate gradient. Ecology 98:1117–1129.
540 https://doi.org/10.1002/ecy.1751

541 Webb SM (2005) SIXpack: a graphical user interface for XAS analysis using IFEFFIT. Phys Scr
542 2005:1011. https://doi.org/10.1238/Physica.Topical.115a01011

543 Webb SM (2011) The MicroAnalysis Toolkit: X-ray fluorescence image processing software.
544 Chicago, Illinois, (USA), pp 196–199

545 Wedin DA, Tilman D (1990) Species effects on nitrogen cycling: a test with perennial grasses.
546 Oecologia 84:433–441. https://doi.org/10.1007/BF00328157

547 Whalen ED, Smith RG, Grandy AS, Frey SD (2018) Manganese limitation as a mechanism for
548 reduced decomposition in soils under atmospheric nitrogen deposition. Soil Biology and
549 Biochemistry 127:252–263. https://doi.org/10.1016/j.soilbio.2018.09.025

550 Zhang Y, Hobbie SE, Schlesinger WH, et al (2024) Exchangeable manganese regulates carbon
551 storage in the humus layer of the boreal forest. Proceedings of the National Academy of
552 Sciences 121:e2318382121. https://doi.org/10.1073/pnas.2318382121

553

9. Figures

Fig. 1. A) Grass litter manganese **(**Mn) concentrations in initial and 5-month decomposed litter. Litter 1 (L1), Litter 2 (L2), and Litter 3 (L3) reflect litter collected from sites 1, 2, and 3. Hollow columns symbolize initial (freshly senesced) litter Mn concentrations; gray columns symbolize litter decomposition in Site 1; and black columns symbolize decomposition in Site 2. No Mn data are shown for 12-month decompositions or for Site 3 5-month decompositions due to insufficient decomposed litter from these groups. B) Particle density analyses of micro-X-ray absorption spectroscopy (μXAS) images (Figure S4). Columns indicate the relative percentages of Mn oxidation states found on the litter surfaces. White columns symbolize the percentage of Mn^{2+}, gray columns Mn^{3+}, and black columns Mn^{4+}. Initial (freshly senesced) grass litter is designated by *i*. S1, S2, and S3 designate litter decomposed for 12 months in sites 1, 2, and 3. C) Percent mass loss of litter over 5-month decomposition experiment; D) percent mass loss of litter over 12-month decomposition experiment. L1, L2, and L3 show litter collected from sites 1, 2, and 3; S1, S2, and S3 designate litter decomposed in sites 1, 2, and 3. Letters above columns define statistically significant differences among litter types at $p \leq 0.05$, n = 2–5. Error bars indicate standard error of the mean (SEM).

Fig. 2. A) Variation in percent mass loss of litter at 5 months versus litter Mn concentration, B) at 12 months versus litter Mn concentration, C) at 5 months versus soil Mn concentration, D) at 12 months versus soil Mn concentration, E) at 5 months versus mean annual precipitation (MAP), and F) at 12 months versus MAP. Dotted lines show linear trendlines for each plot; the equation and coefficient of determination (R^2) for each line is shown in the top right corner of each plot.

Fig. 3. Micro-X-ray absorption spectroscopy (μXAS) analyses of litter types (A–D) and aggregate litter per condition (E–F); source μXAS images are shown in Figure S6. Element concentrations are measured as photon counts per image pixel, or the signal intensity of the target oxidation state of manganese (Mn) in the X-ray images' regions of interest. A) White boxes and circles represent Mn^{2+} percentages, B) gray boxes and circles Mn^{3+}, and C) black boxes and circles Mn^{4+}. *C1*, *C2*, and *C3* are the control litter groups, and *MnT1*, *MnT2*, and *MnT3* are the Mn-treatment litter groups; numbers (1, 2, and 3) indicate the respective litter-collection site. D, F) White columns represent Mn^{2+} percentages, gray columns Mn^{3+}, and black Mn^{4+}. E) Hollow boxes and circles represent litter in the control condition, and gray boxes and circles show litter under Mn treatment. In A–C and E, the middle line in each box represents the median, the bottom and top lines represent 1st and 3rd quartiles, the x represents the mean, and the whiskers extend to the minimum and maximum values; outliers are shown as circles. In D and F) error bars indicate standard error of the mean (SEM). Asterisks define significant differences A–D) among litter types or E–F) between treatments at $p \leq 0.05$; brackets show paired comparisons.

Fig. 4. Percent mass loss in litter incubated for 10 months. Litter 1 (L1), Litter 2 (L2), and Litter 3 (L3) reflect litter collected from sites 1, 2, and 3. Hollow columns and black-filled columns represent control and manganese- (Mn) treatment litter, collected from sites 1 (the driest), 2, and 3 (the wettest). Hollow boxes and black-filled boxes represent aggregated control and Mn-treatment litter, respectively. Control and Mn-treatment litter are compared by A) litter type (collection site) and by B) aggregated condition. No significant differences were found A)

among litter type or B) between condition ($p \leq 0.05$, $n = 3$ per litter type, $n = 9$ per condition). Error bars indicate standard error of the mean (SEM). Boxplots show means (X) and inclusive quartiles.

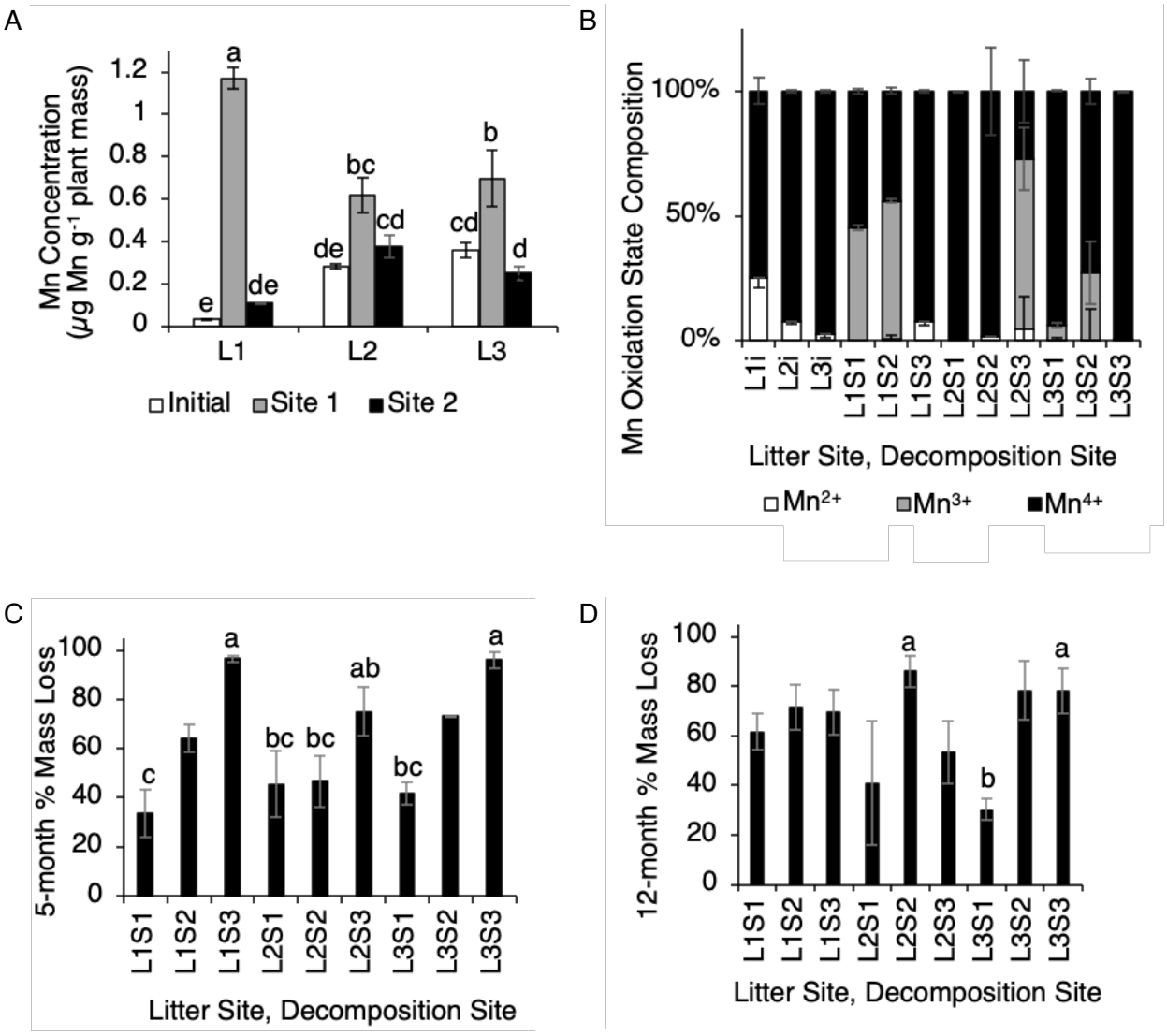
A
Mn Concentration (μg Mn g-1 plant mass)
1.2
1
0.8
0.6
0.4
0.2
0
a
e
de
bc
de
cd
b
cd
d
L1
L2
L3
Initial
Site 1
Site 2
B
Mn Oxidation State Composition
100%
50%
0%
L1i
L2i
L3i
L1S1
L1S2
L1S3
L2S1
L2S2
L2S3
L3S1
L3S2
L3S3
Litter Site, Decomposition Site
Mn2+
Mn3+
Mn4+
C
5-month % Mass Loss
100
80
60
40
20
0
c
a
bc
bc
ab
bc
a
L1S1
L1S2
L1S3
L2S1
L2S2
L2S3
L3S1
L3S2
L3S3
Litter Site, Decomposition Site
D
12-month % Mass Loss
100
80
60
40
20
0
a
b
a
L1S1
L1S2
L1S3
L2S1
L2S2
L2S3
L3S1
L3S2
L3S3
Litter Site, Decomposition Site

Fig. 1

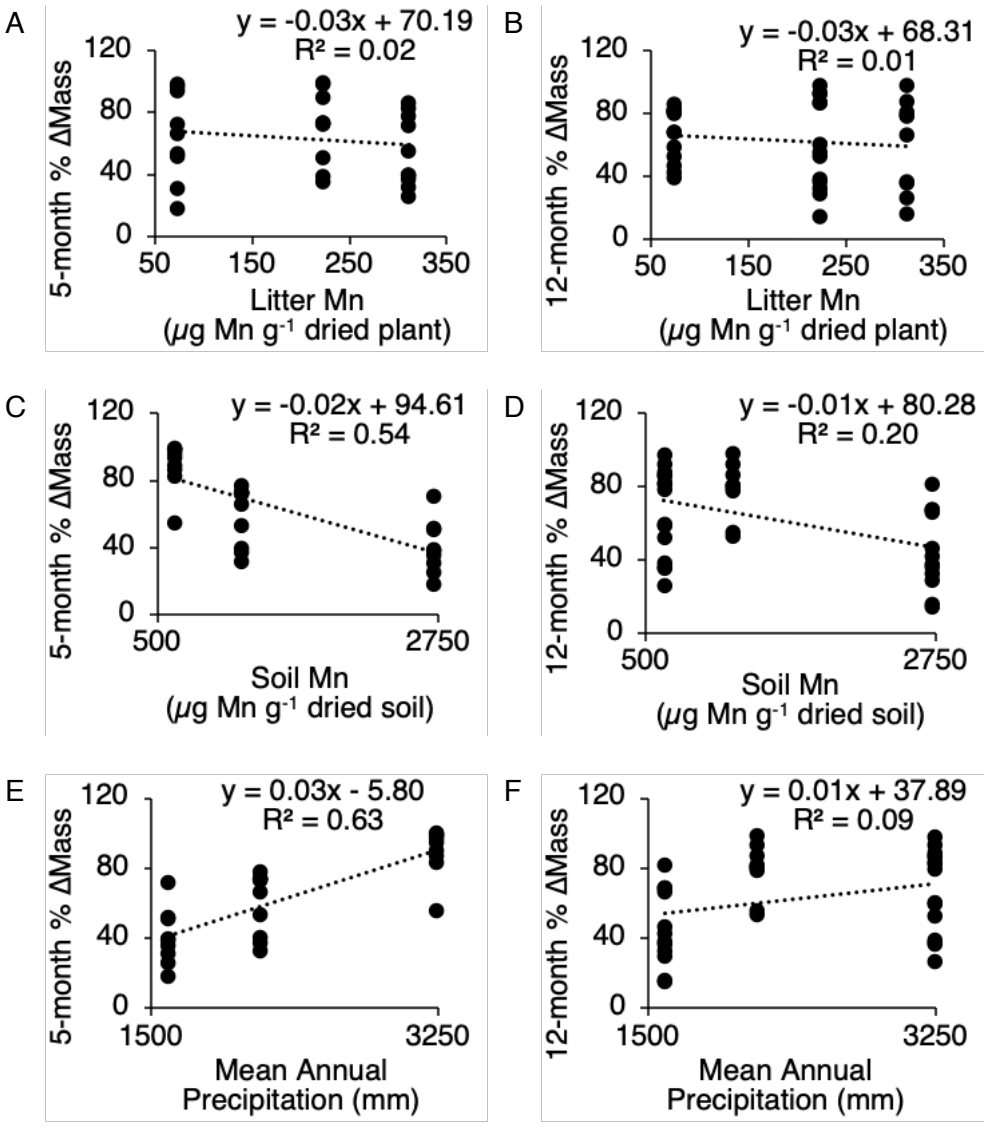
A
y = -0.03x + 70.19
R² = 0.02
5-month % ΔMass
120
80
40
0
50
150
250
350
Litter Mn
(μg Mn g-1 dried plant)
B
y = -0.03x + 68.31
R² = 0.01
12-month % ΔMass
120
80
40
0
50
150
250
350
Litter Mn
(μg Mn g-1 dried plant)
C
y = -0.02x + 94.61
R² = 0.54
5-month % ΔMass
120
80
40
0
500
2750
Soil Mn
(μg Mn g-1 dried soil)
D
y = -0.01x + 80.28
R² = 0.20
12-month % ΔMass
120
80
40
0
500
2750
Soil Mn
(μg Mn g-1 dried soil)
E
y = 0.03x - 5.80
R² = 0.63
5-month % ΔMass
120
80
40
0
1500
3250
Mean Annual
Precipitation (mm)
F
y = 0.01x + 37.89
R² = 0.09
12-month % ΔMass
120
80
40
0
1500
3250
Mean Annual
Precipitation (mm)

Fig. 2

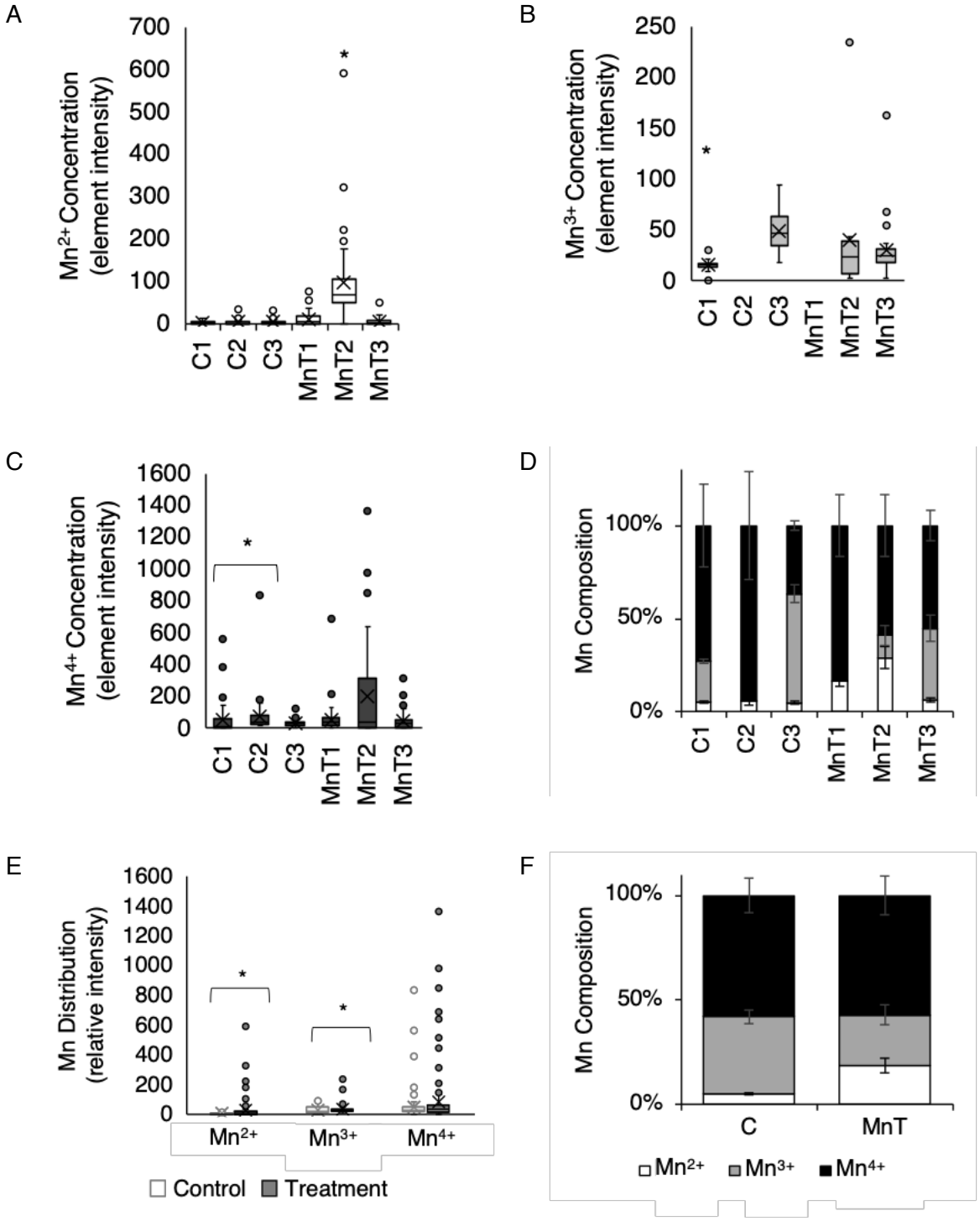
A
Mn2+ Concentration (element intensity)
700
600
500
400
300
200
100
0
C1
C2
C3
MnT1
MnT2
MnT3
B
Mn3+ Concentration (element intensity)
250
200
150
100
50
0
C1
C2
C3
MnT1
MnT2
MnT3
C
Mn4+ Concentration (element intensity)
1600
1400
1200
1000
800
600
400
200
0
C1
C2
C3
MnT1
MnT2
MnT3
D
Mn Composition
100%
50%
0%
C1
C2
C3
MnT1
MnT2
MnT3
E
Mn Distribution (relative intensity)
1600
1400
1200
1000
800
600
400
200
0
Mn2+
Mn3+
Mn4+
Control
Treatment
F
Mn Composition
100%
50%
0%
C
MnT
Mn2+
Mn3+
Mn4+

Fig. 3

A

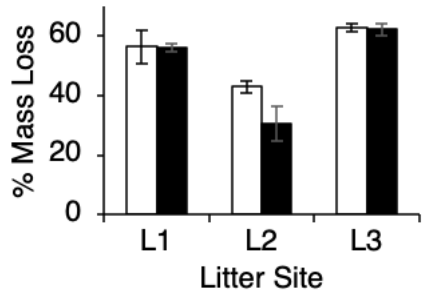
% Mass Loss
60
40
20
0
L1
L2
L3
Litter Site

B

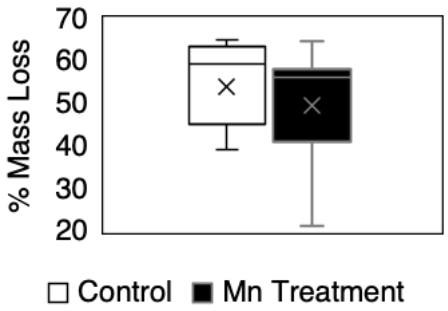
% Mass Loss
70
60
50
40
30
20
Control
Mn Treatment

Fig. 4

10. Supplementary Figures

Fig. S1. Field sites arrayed along a 14-km transect on the Kohala rainfall gradient, Island of Hawaii. Mean annual precipitation (MAP) varies from <300 to >3200 mm. Google Earth map and inset of the Island of Hawaii display the locations of field sites, represented by numbered white dots.

Fig. S2. Total manganese (Mn) concentrations in A) soil and B) grass litter in 46 sites along the Kohala gradient. Soil and grass Mn concentrations were measured using X-ray fluorescence (XRF). Soils were sampled as continuous 10-cm soil cores, manually homogenized, and sieved to 2 mm. Grasses were cut at their bases to limit collection to aboveground mass. Samples were collected in the summers of 2018 and/or 2019 and were measured in at least triplicate (n = 3–6). Error bars symbolize the standard error of the mean (SEM).

Fig. S3. A) Representative litter bag used in the field and laboratory experiments. Litter bags were constructed from 6cm x 12cm sections of 0.011-gauge fiberglass insect screen cloth folded in half lengthwise and secured by ribbon sewn onto three sides of the resulting 6-cm^2 square. B) Experimental setup for the 10-month laboratory experiment. The control (left bin) and manganese- (Mn) treatment (right bin) conditions received weekly additions of 495 ml of deionized (DI) water (no additional manganese [Mn]) or 17.6μM manganese chloride ($MnCl_2$), respectively, to approximate the average daily rainfall of the wettest site, dispersed across the soil substrate and surface area of the incubation container's bottom. Litter bags are clipped together according to litter collection site (1, 2, or 3). C–F) We observed fungal hyphae while inspecting litter bags at the completion of the 10-month incubation. White arrows indicate the locations of suspected fungal hyphae C, E) through the mesh of the litter bag and D, F) in the open litter bag. Views of the same litter bag collected from Site 3: C) sealed and D) opened. Views of the same litter bag collected from Site 2: E) sealed and F) opened.

Fig. S4. Miro-X-ray fluorescence (μXRF) imagery of manganese (Mn) oxidation states distributed across grass litter surfaces. Litter types are identified by the text under each respective image: A) Initial Site 1 (freshly senesced litter collected from Site 1); B) Initial Site 2; C) Initial Site 3; D) Litter 1, Site 1 (litter collected from Site 1 and decomposed in Site 1); E) Litter 1, Site 2; F) Litter 1, Site 3; G) Litter 2, Site 1; H) Litter 2, Site 2; I) Litter 2, Site 3; J) Litter 3, Site 1; K) Litter 3, Site 2; L) Litter 3, Site 3. Regions where Mn^{2+} was detected are shown in blue, Mn^{3+} in green, and Mn^{4+} in red. Regions of green-red overlap indicate areas of $Mn^{3+/4+}$ oxides and litter-decomposition hot spots.

Fig. S5. Carbon-to-nitrogen ratios (C/N) in grass litter over A) 5-month and B) 12-month decompositions. No statistically significant differences ($p \leq 0.05$, n = 2–5) were found within the 5-month or 12-month decompositions. Error bars indicate standard error of the mean (SEM). Litter 1, Litter 2, and Litter 3 reflect litter collected from sites 1, 2, and 3. Site 1, Site 2, and Site 3 designate litter decomposed in sites 1, 2, and 3.

Fig. S6. Miro-X-ray fluorescence (μXRF) imagery of manganese (Mn) oxidation states distributed across grass litter surfaces. Litter treatment conditions are identified by the text in the columns to the right of each image: A) Control 1, B) Control 2, C) Control 3, D) Mn Treatment 1, E) Mn Treatment 2, F) Mn Treatment 3. Regions where Mn^{2+} was detected are shown in blue, Mn^{3+} in green, and Mn^{4+} in red. Regions of green-red overlap indicate areas of $Mn^{3+/4+}$ oxides and litter-decomposition hot spots. The consolidated bright red lines in panel D) may suggest fungal hyphae colonizing the litter surface.

Fig. S7. Changes in carbon-to-nitrogen ratios (C/N) in litter incubated for 10 months. L1, L2, and L3 reflect litter collected from sites 1, 2, and 3. Hollow columns and black-filled columns represent control and manganese- (Mn) treatment litter, collected from sites 1, 2, and 3. Hollow boxes and black-filled boxes represent aggregated control and Mn-treatment litter. No significant differences were found between control and Mn-treatment litter when we compared them by litter type (collection site) (A) or by aggregated condition (B). Letters above columns indicate significant categories ($p \leq 0.05$, $n = 3$ per litter type, $n = 9$ per condition), and error bars indicate standard error of the mean (SEM). Boxplots show means (X) and inclusive quartiles.

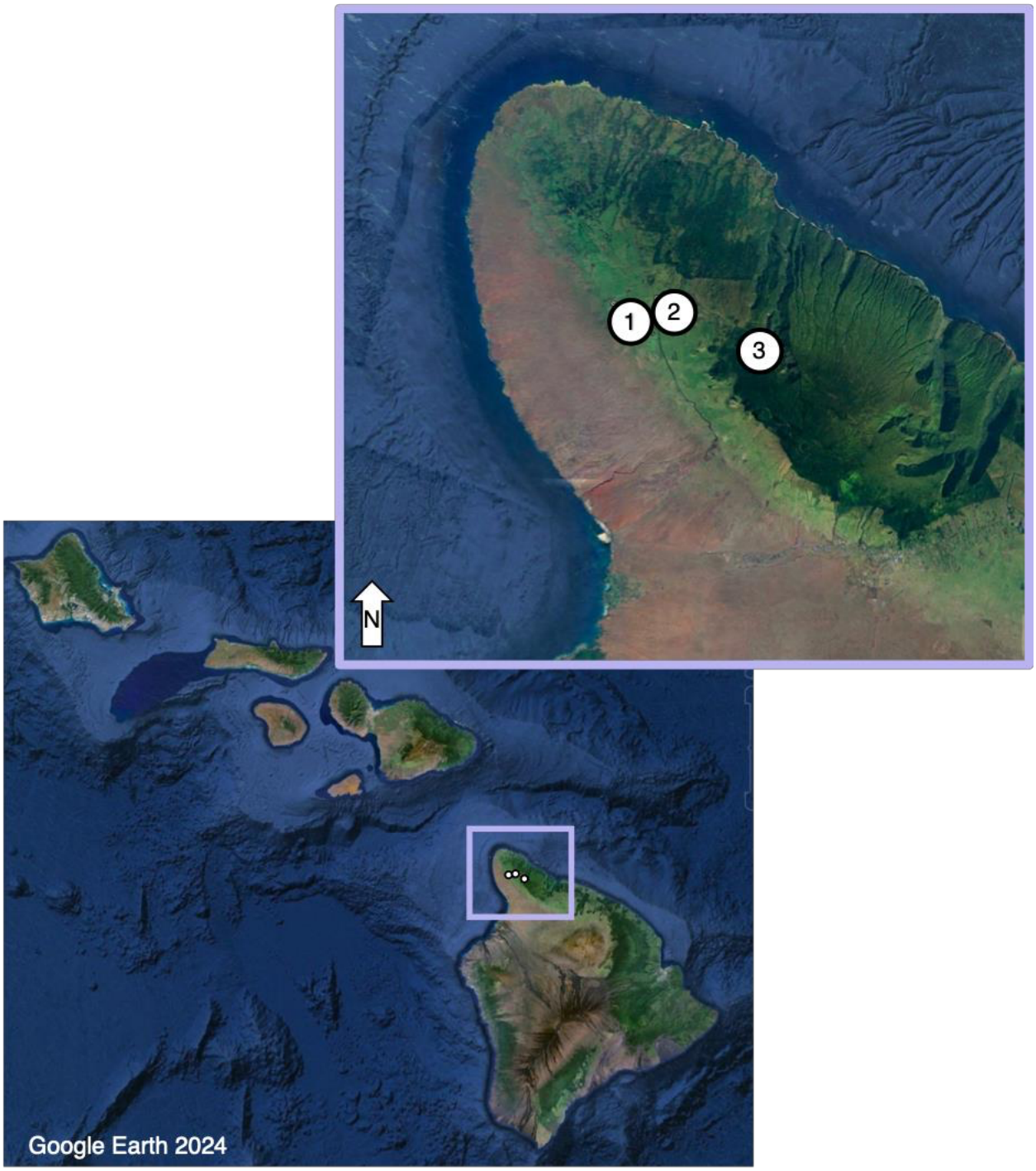

Fig S1

A

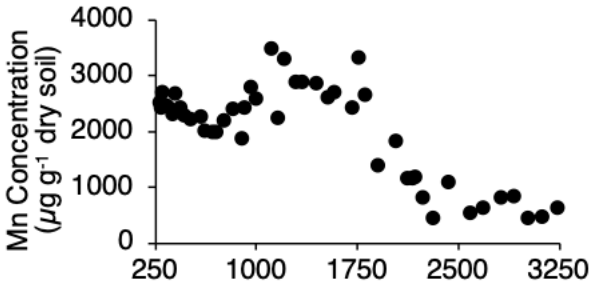
Mn Concentration
(μg g-1 dry soil)
4000
3000
2000
1000
0
250
1000
1750
2500
3250

B

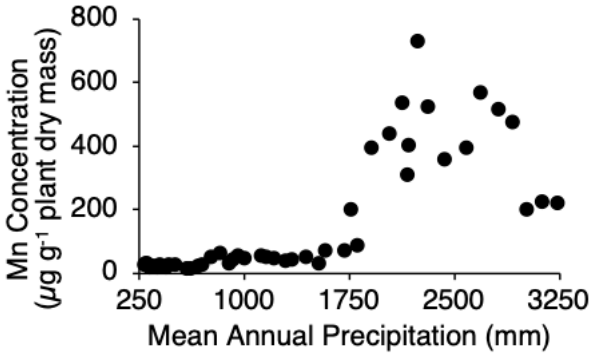
Mn Concentration
(μg g-1 plant dry mass)
800
600
400
200
0
250
1000
1750
2500
3250
Mean Annual Precipitation (mm)

Fig. S2

Fig. S3

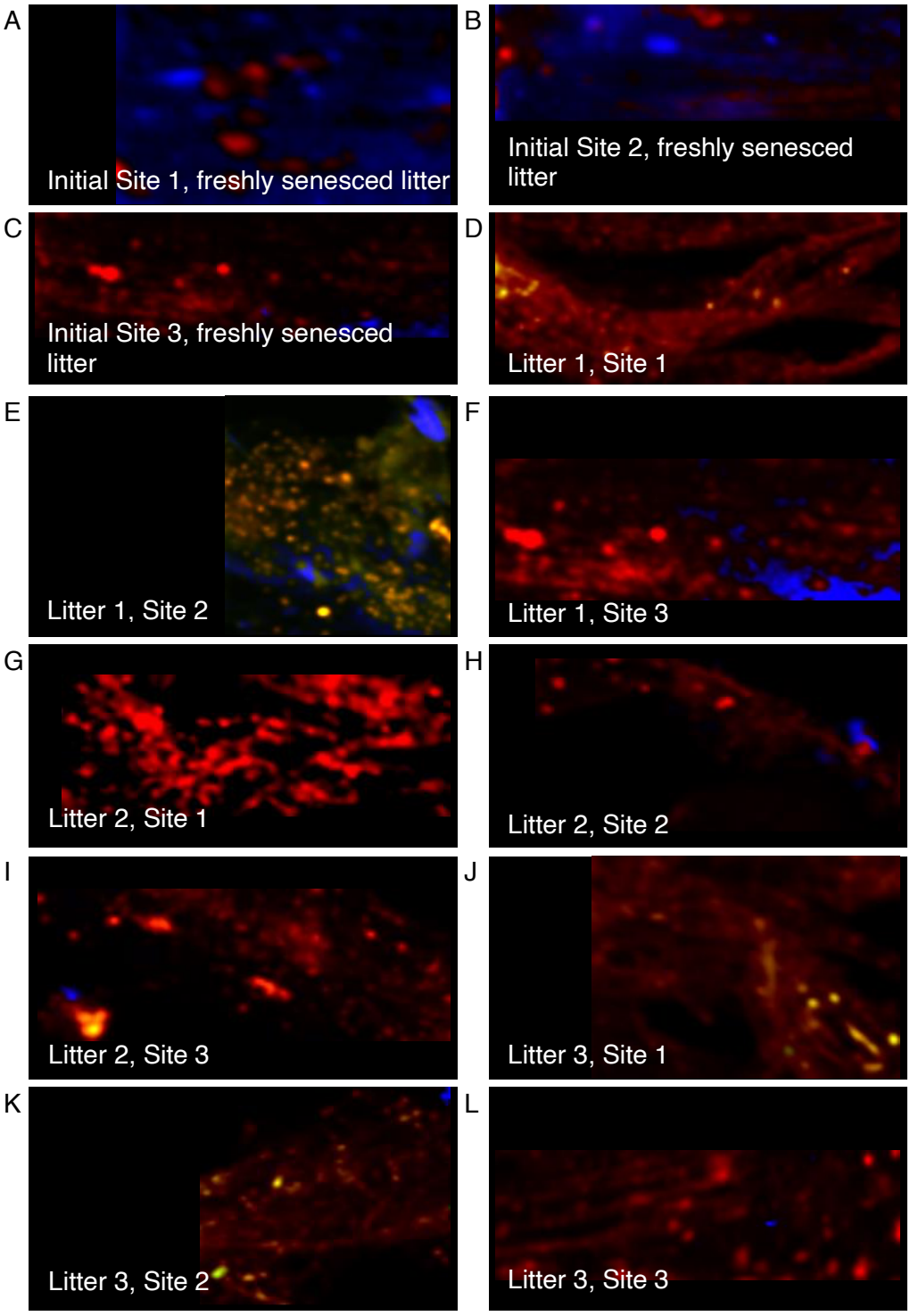
A
Initial Site 1, freshly senesced litter
B
Initial Site 2, freshly senesced litter
C
Initial Site 3, freshly senesced litter
D
Litter 1, Site 1
E
Litter 1, Site 2
F
Litter 1, Site 3
G
Litter 2, Site 1
H
Litter 2, Site 2
I
Litter 2, Site 3
J
Litter 3, Site 1
K
Litter 3, Site 2
L
Litter 3, Site 3

Fig. S4

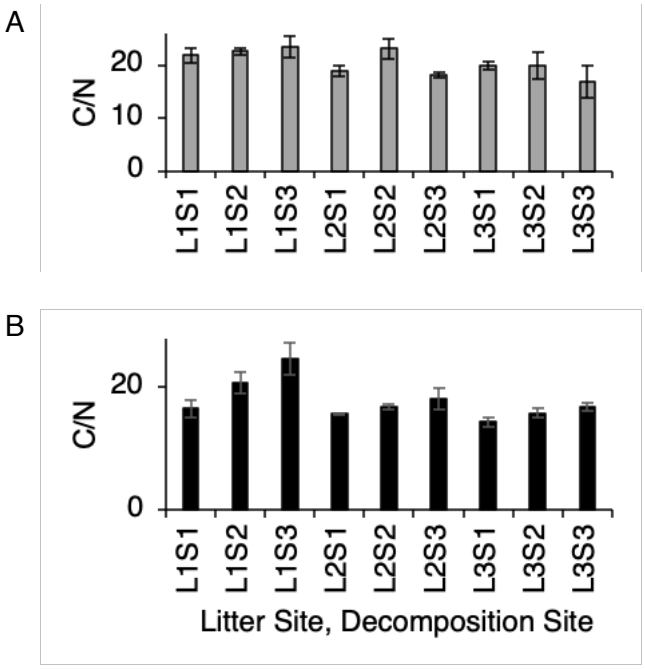
A
C/N
20
10
0
L1S1
L1S2
L1S3
L2S1
L2S2
L2S3
L3S1
L3S2
L3S3
B
C/N
20
0
L1S1
L1S2
L1S3
L2S1
L2S2
L2S3
L3S1
L3S2
L3S3
Litter Site, Decomposition Site

Fig. S5

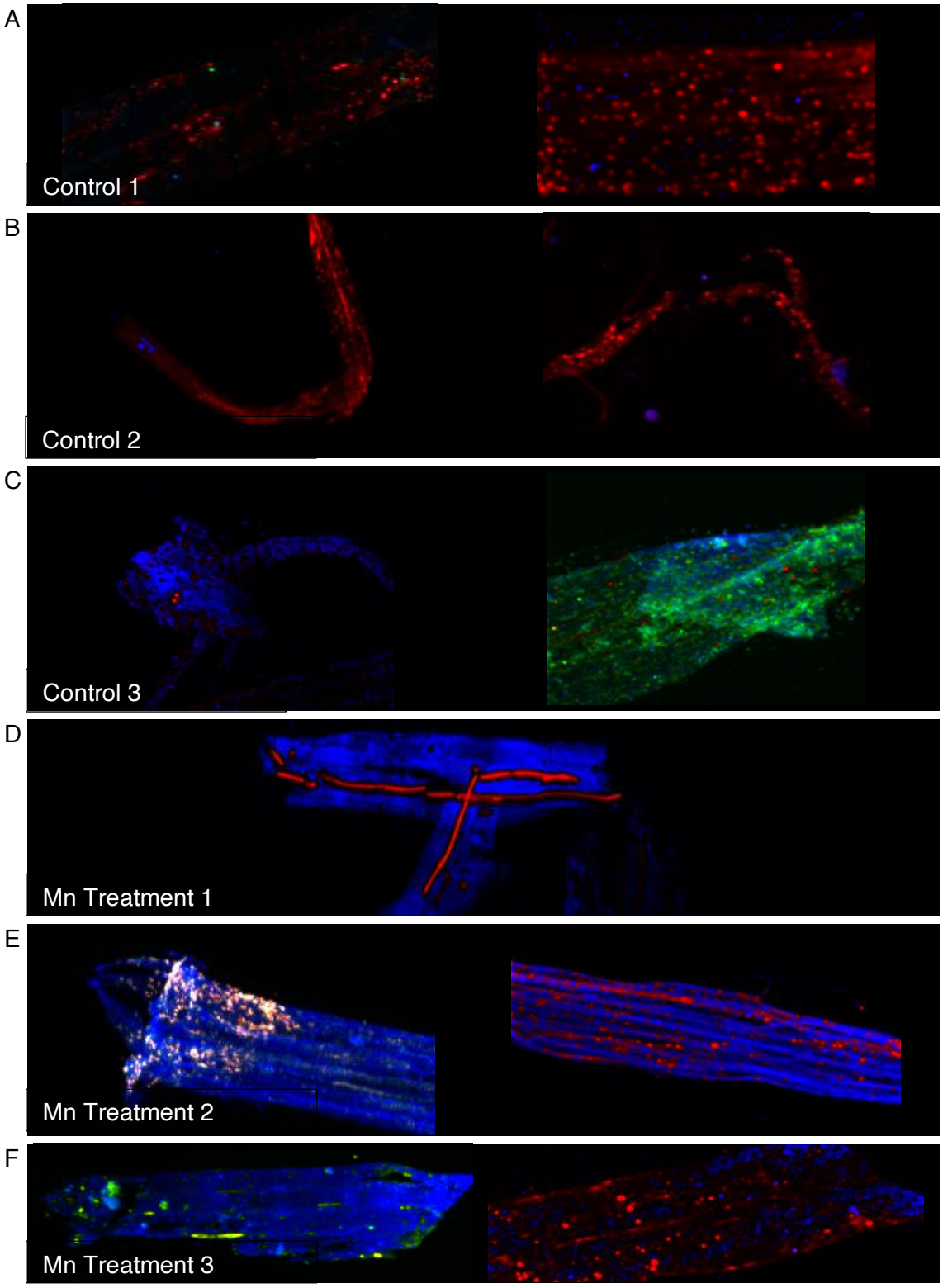
A
Control 1
B
Control 2
C
Control 3
D
Mn Treatment 1
E
Mn Treatment 2
F
Mn Treatment 3

Fig. S6

A

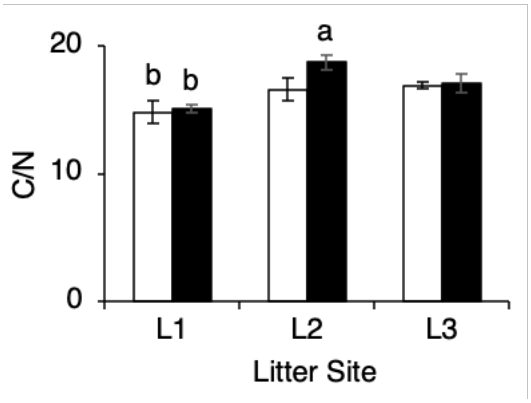
20
10
0
C/N
b
b
a
L1
L2
L3
Litter Site

B

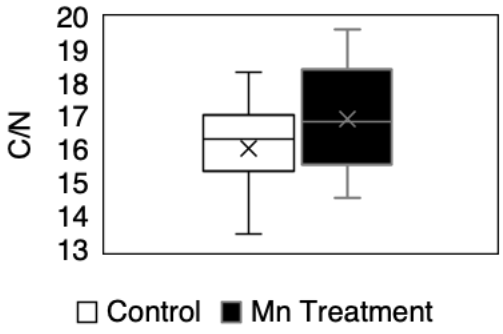
20
19
18
17
16
15
14
13
C/N
Control
Mn Treatment

Fig. S7